Electronic Supplementary Information

Low-voltage organic single-crystal field-effect transistors and inverters enabled by a solution processable high-*k* dielectric

Chunli Ma,[‡a] Bin Li,[‡a] Yihan Zhang,[‡a] Jiamin Wang,[a] Ying Liu,[a] Lingjie Sun,[a,b] Xinzi Tian,[a] Jiarong Yao,[a] Zhaofeng Wang,[a] Shuyu Li,[a] Fangxu Yang,[*a] Rongjin Li,[*a] and Wenping Hu[a,b]

[a.] Tianjin Key Laboratory of Molecular Optoelectronic Sciences, Department of Chemistry, School of Science, Tianjin University, Tianjin 300072, China. E-mail: yangfangxu@tju.edu.cn, lirj@tju.edu.cn.

[b.] Joint School of National University of Singapore and Tianjin University, Fuzhou International Campus of Tianjin University, Binhai New City, Fuzhou, 350207, China.

1. Table S1 to S3

Table S1 Mobility comparison of recently reported low-voltage OFETs based on high-*k* dielectrics and OTS-modified SiO_2 dielectrics for the same semiconductor, respectively.

Ref.[a]	Dielectric	OSC	μ [$cm^2\ V^{-1}\ s^{-1}$)]	μ_0 [$cm^2\ V^{-1}\ s^{-1}$)]	Mobility reduction	Ref.[b]
1	AlO_x/C14 PA	DPA	1.2	34	96.5 %	10
2	TiO_x	Pentacene	0.12	3	96.0 %	11
3	AlO_x	C10-DNTT	1.8	8	98.0 %	12
4	AlO_x/PS	C8-BTBT	3.8	8.7	56.3 %	13
5	$ZrTiO_x$/PS	Pentacene	0.55	3	81.7 %	11
7	HfO_2/COC	PTCDI-C13	0.27	2.1	87.1 %	14
7	HfO_2/COC	Pentacene	0.47	3	84.3 %	11
8	HfO_2/π-σ PA	Pentacene	0.22	3	92.7 %	11
9	ZrO_x/PαMS	Pentacene	0.51	3	83.0 %	11
This work	HAO/ODPA	C6-DPA	3.0	3.16	5.1 %	15

[a] References based on high-*k* dielectrics.

[b] References based on SiO_2 dielectric.

μ_0: Comparative mobility, i.e., mobility calculated from OFETs based on OTS/SiO_2 dielectrics

μ: Mobility calculated from OFETs based on high-*k* dielectrics

Mobility reduction: $(\mu_0-\mu)/\ \mu_0*100\%$

Table S2 Comparison of electrical characteristics of recently reported low voltage OFETs based on high-*k* dielectrics.

Ref.	Dielectric	Method	OSC	*SS* [mV dec^{-1}]	μ [$cm^2 V^{-1} s^{-1}$]	On/Off Ratio	D_{it} [$\times 10^{-11}$ $eV^{-1}cm^{-2}$)]
1	AlO_x/SAM	Anodization	DPA	66	1.2	4×10^6	2.09
2	TiO_x	Sol-Gel	Pentacene	180	0.12	10^4	76.1
3	AlO_x	Sol-Gel	C10-DNTT	110	1.8	10^5	9.65
4	AlO_x/PS	Anodization	C8-BTBT	107	1.53	10^8	8.78
5	$ZrTiO_x$/PS	Sol-Gel	Pentacene	510	0.55	10^4	52.3
6	HfO_2/SAM	Sol-Gel	PDPP2DT-T2	230	1.16	$7\times10_4$	114
7	HfO_2/COC	Sol-Gel	Pentacene	450	0.47	$6\times10_4$	45.8
7	HfO_2/COC	Sol-Gel	PTCDI-C13	310	0.27	$4\times10_3$	36.4
8	HfO_2/SAM	Sol-Gel	Pentacene	100	0.22	10^6	29.7
9	ZrO_x/PαMS	Sol-Gel	Pentacene	260	0.51	1.2×10^5	37.3
This work	HAO/SAM	Sol-Gel	C6-DPA	60	3.0	10^7	0.181

Table S3 Comparison of the performances of recently reported organic inverters operating at low voltages.

Ref.	Dielectric	OSC (p-type, n-type)	Operating voltage (V)	Gain
16	Hf-SAND	PBTOR, P(NDI2OD-T2)	4	38
17	pV3D3	DNTT, PTCDI-C13	5	131
18	$HfTiO_x$/SAM	Pentacene, PTCDI-C13	3	6
19	AlO_x/SAM	DNTT, PDI-8CN2	3	63
20	TiO_2/SAM	DNTT, PDI-8CN2	0.9	62
21	AlO_x/SAM	DPh-BTBT, N1100	1	180
22	HfO_2/Polyimide	Pentacene, PTCDI-C13	8	46
23	Parylene-C/PMMA	29-DPP-TVT,P(NDI2OD-T2)	10	13
24	Parylene	diF-TES-ADT:PS,TU-3:PaMS	10	25
25	AlO_x/ PADMA	C_8-DNBDT-NW, PhC_2-BQQDI	1	66
26	Al_2O_3 /TMSC	Pentacene, C60	4	500
27	C nanoparticles (NPs)/PS	Pentacene, PTCDI-C13H27	1.5	500
28	Ta_2O_5	Pentacene, PTCDI-C13	5	500
29	AlO_x/SAM	DNTT, Compound 8	3	370
This work	HAO/SAM	C6-DPA, TFT-CN	4	172

2. Figure S1 to S14

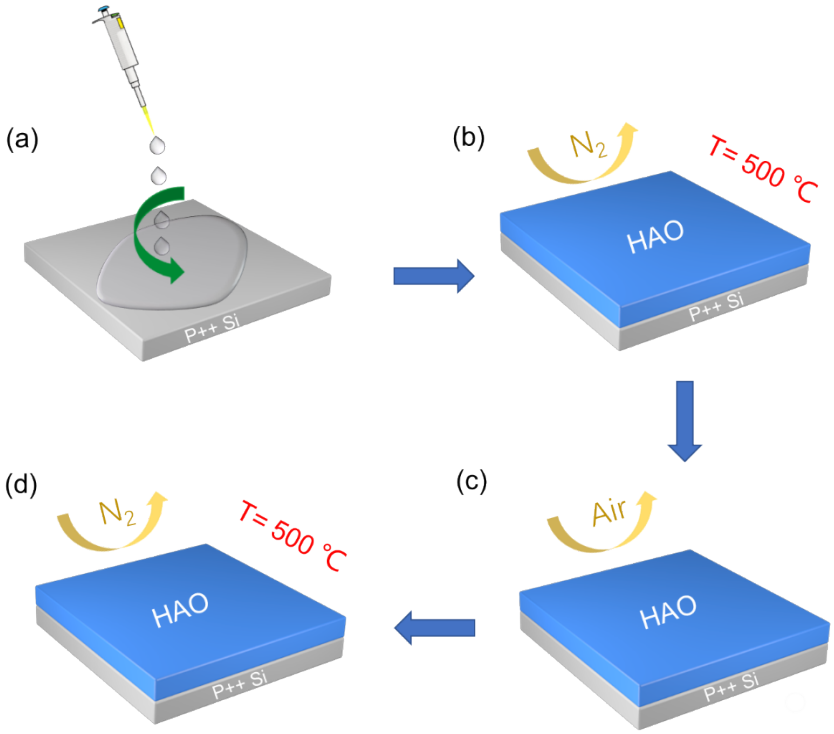

Fig. S1 (a-d) The annealing of the HAO dielectrics by a "Nitrogen-Air-Nitrogen (NAN)" process.

After spin coating (Fig. S1(a)), a finely designed annealing process was used to optimize the quality of the binary metal oxide dielectric film. First, a low-temperature pre-annealing process was introduced to remove the most solvent, which prevents the volatilization process from affecting the densification process of the film. After this, the film was raised to the annealing temperature in a nitrogen atmosphere within a short of time (30 min) (Fig. S1(b)). Next, the air was deliberately introduced and kept for a while (Fig. S1(c)), then it was changed back to the nitrogen (Fig. S1(d)) and naturally cooled to room temperature. For comparison, another dielectric was prepared, whose annealing process was all carried out in nitrogen.

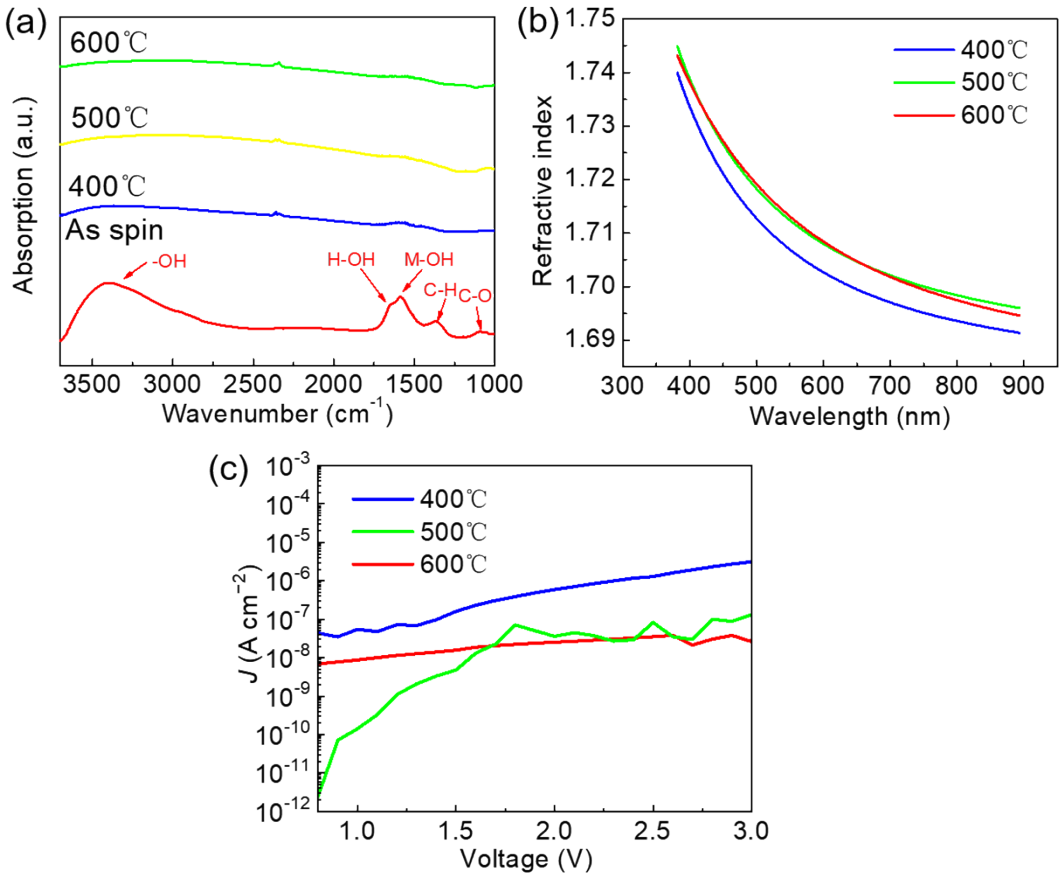

Fig. S2 (a) FT-IR spectrum of the HAO dielectric prepared by the NAN process with different annealing temperatures. (b) Refractive index of the HAO dielectric processed by the NAN process with different annealing temperatures. (c) Leakage current density of the HAO dielectric processed by the NAN process with different annealing temperatures.

FT-IR data was presented in Fig. S2(a). For the as-spun films, the broad band centered at 3400 cm^{-1}, the shoulder at 1650 cm^{-1}, and the peak at 1590 cm^{-1} are assigned to O-H stretch vibrations associated with hydroxyl groups, the H-OH bending vibration of adsorbed water in the films, and the M-OH stretching vibration, respectively. M stands for Hf or Al. The CH_3 present in the as-spun film at, 1365 cm^{-1}, is likely from adsorbed solvent and organic ligand in the HAO dielectric layer. These absorption bands were significantly suppressed or eliminated by annealing at 400°C and above. The refractive index of dielectrics was measured by spectroscopic ellipsometry (Fig. S2(b)), and the refractive index can reflect its density. It showed that the film density was improved as the annealing temperature increased, and the HAO dielectric layer annealed at 500°C and 600°C exhibited similar density. The same phenomenon was also shown in the leakage current curves processed by different annealing temperatures (Fig. S2(c)). When the annealing temperature reached 600°C, the leakage current was not further reduced[30].

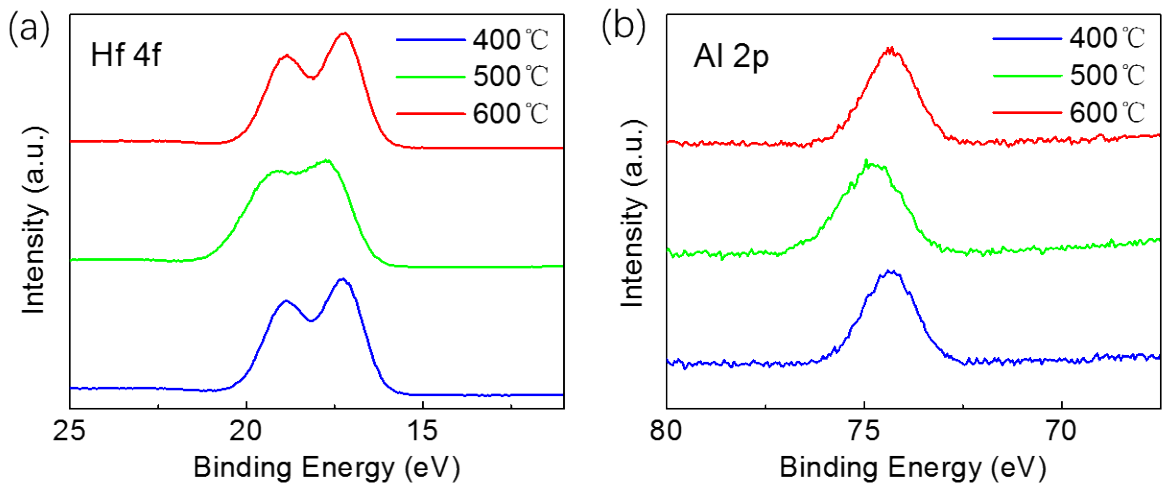

Fig. S3 (a) Hf 4f XPS spectrum of the HAO dielectric treated by NAN process with different annealing temperatures. (b) Al 2p XPS spectrum of the HAO dielectric treated by NAN process with different annealing temperatures.

To obtain more information on chemical bonding states from HAO dielectrics, the evolution of the Hf 4f core-level XPS spectra related to different annealing temperatures were investigated, as shown in Fig. S3. With the increase of annealing temperature, the doublet peaks corresponding to Hf 4f5/2 and Hf 4f7/2 shifted towards higher binding energy sides, indicating the formation of Hf-Al-O. However, When the annealing temperature was increased to 600°C, the binding energy of the Hf 4f peak was detected to shift to the low energy side, which may be due to the decomposition of $HfAlO_x$ and the partial formation of HfO_X. The same trend was also observed for Al 2p core-level XPS spectrum.[27,28] Thus, 500°C was adopted as the annealing temperature.

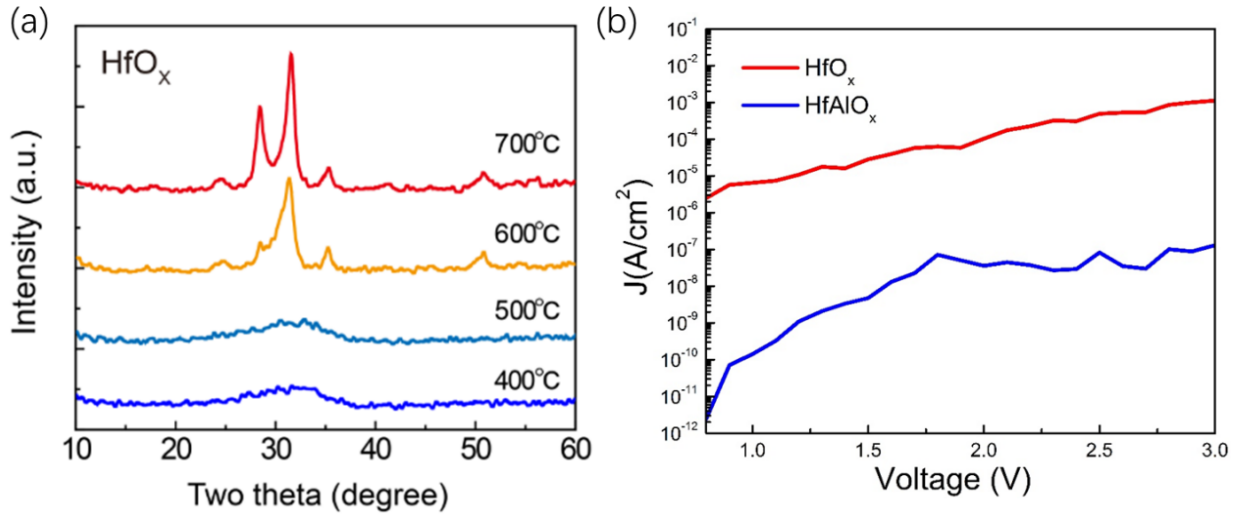

Fig. S4 (a) XRD patterns of the HfO_x dielectric at different annealing temperatures. (b) Comparison of the leakage current of the HfO_x and HAO dielectric.

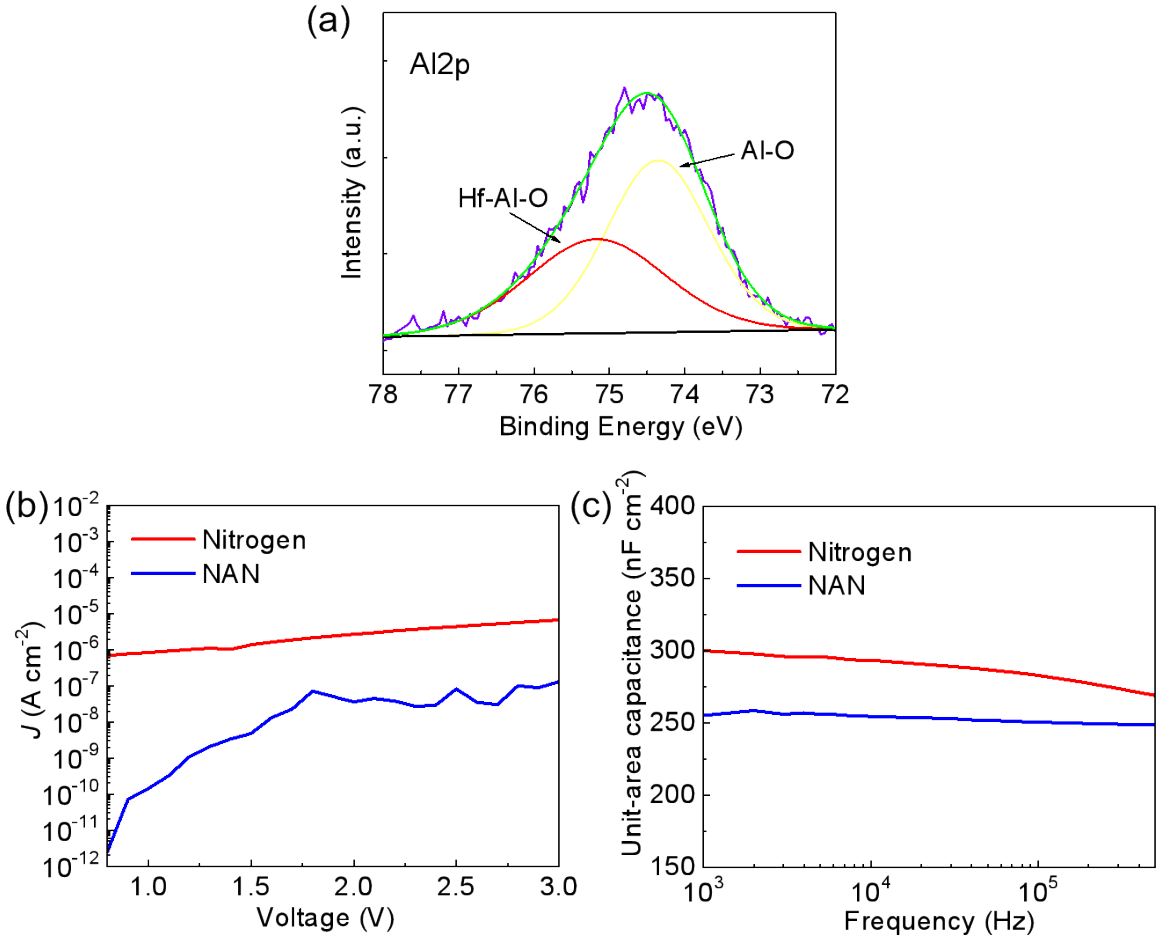

Fig. S5 (a) Al 2p XPS spectrum of the HAO dielectric treated in nitrogen. (b) Comparison of leakage current of HAO dielectric treated by NAN process and treated in nitrogen. (c) Comparison of unit-area capacitance of HAO dielectric treated by NAN process and treated in nitrogen.

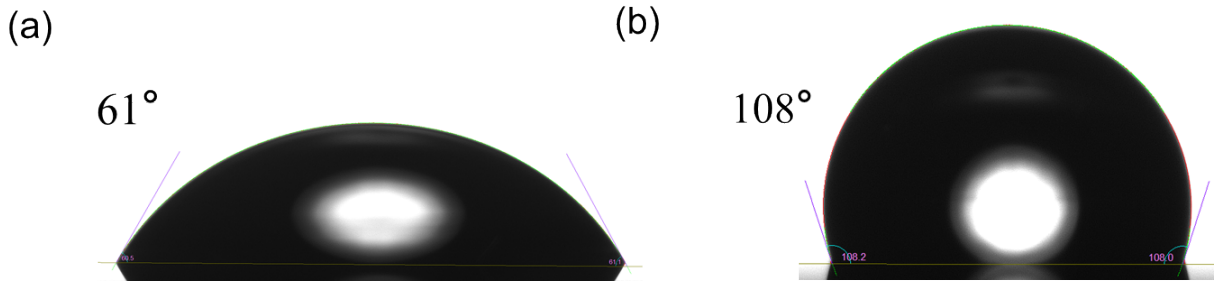

Fig. S6 (a) Water contact angles of the bare-HAO surface. (b) Water contact angles of the SAM/HAO surface.

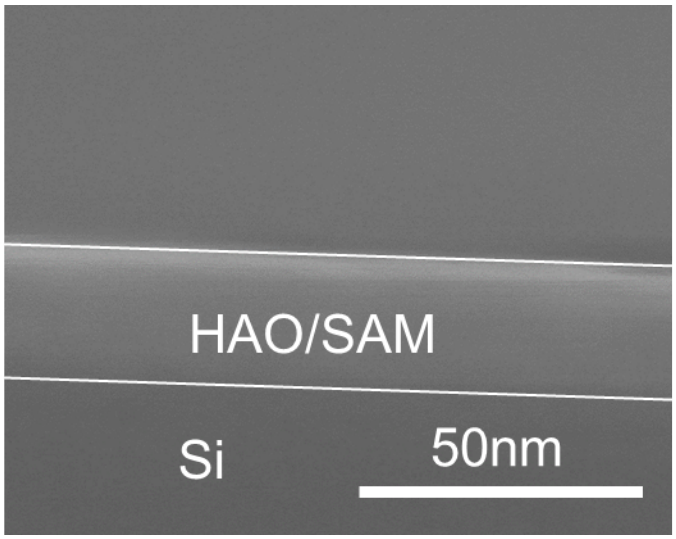

Fig. S7 Cross-section SEM images of the SAM/HAO dielectric.

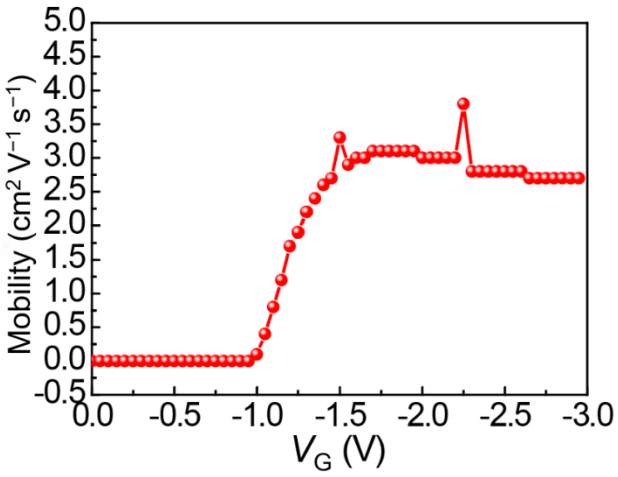

Fig. S8 Carrier mobility as a function of gate bias.The channel length was 135 μm, and the channel width was 180 μm

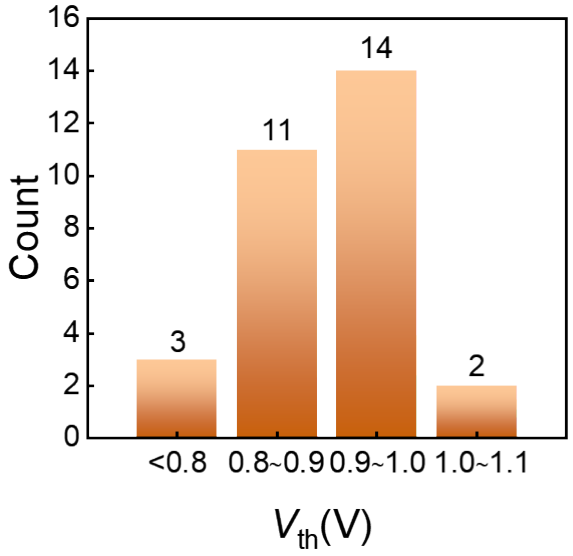

Fig. S9 (a) Histogram of Vth measured from 30 devices. The channel length was 135 μm, and the channel width was 180 μm.

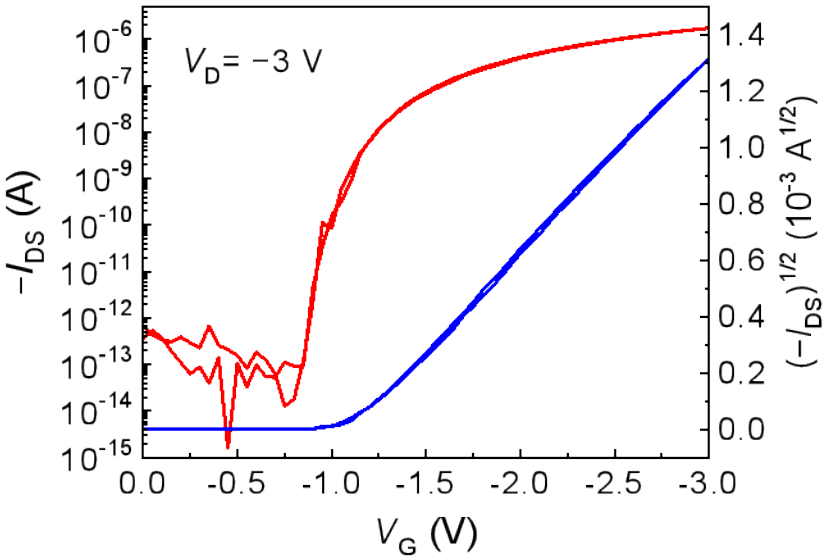

Fig. S10 Hysteresis characteristics of the OFETs based on C6-DPA 2DMCs and SAM/HAO dielectrics. The channel length was 135 μm, and the channel width was 180 μm.

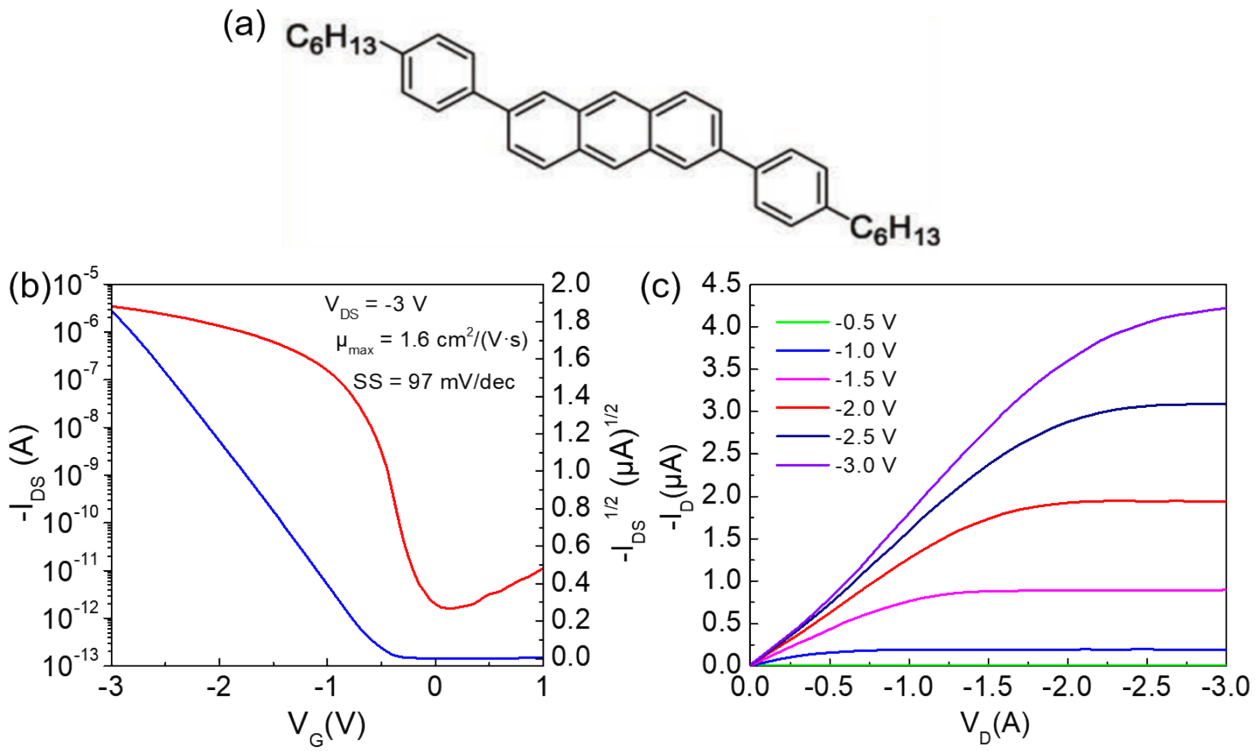

Fig. S11 (a) Chemical structure of C6-DPA. (b, c)Typical transfer and output characteristics of the OFETs based on C6-DPA 2DMCs and SAM/HAO dielectrics whose bonding mode is not controlled. The channel length was 55 μm, and the channel width was 190 μm.

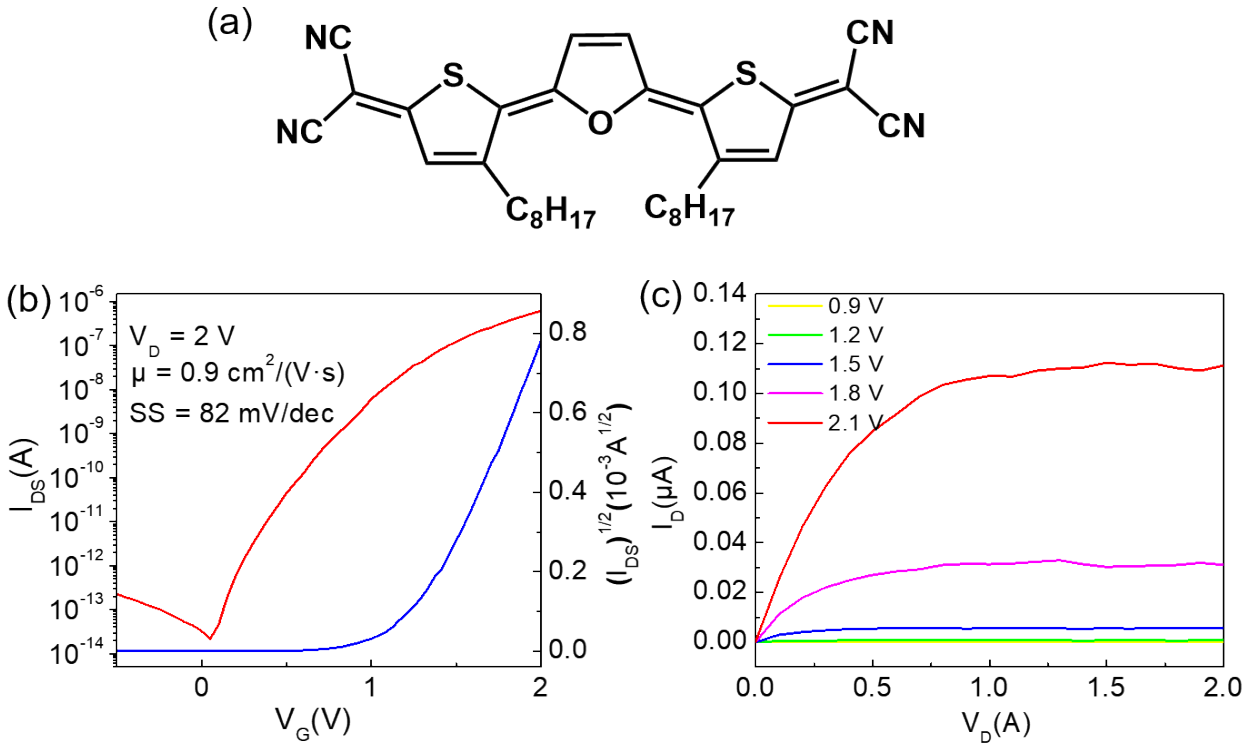

Fig. S12 (a) Chemical structure of TFT-CN. (b, c) Typical transfer andoutput characteristics of the OFETs based on TFT-CN 2DMCs and SAM/HAO dielectrics. The channel length was 40 μm, and the channel width was 200 μm.

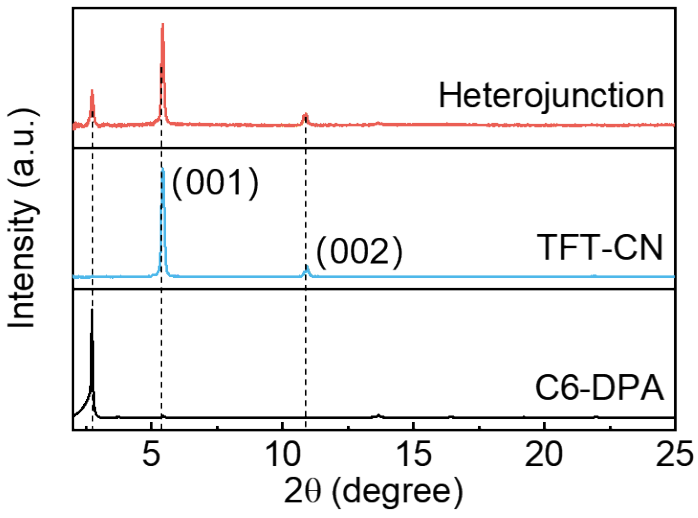

Fig. S13 XRD patterns of 2DMCs of C6-DPA, TFT-CN, and their p-n heterojunctions.

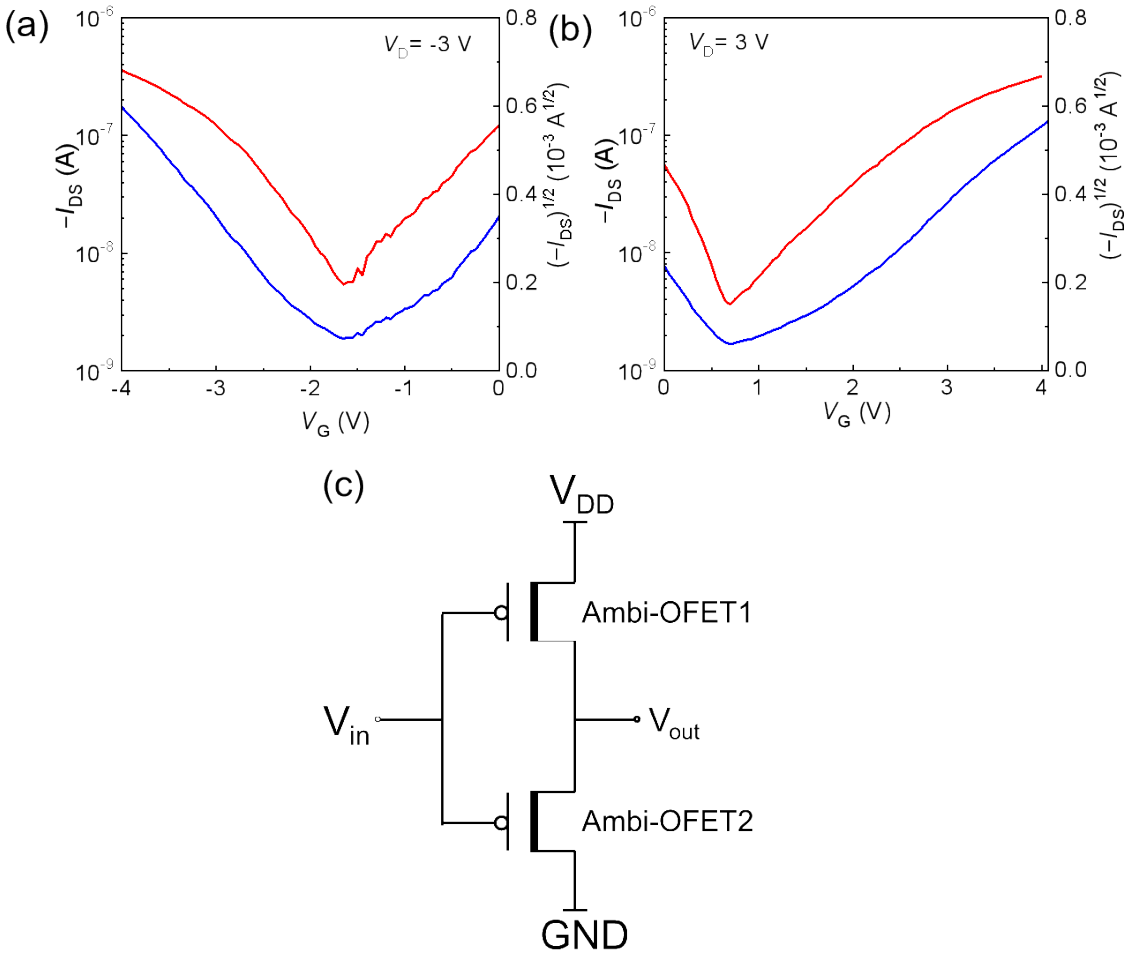

Fig. S14 (a) Typical transfer curves in the p-channel operation mode of the aOFET. (b) Typical transfer curves in the n-channel operation mode of the aOFET. (c) The circuit schematic of the complementary-like inverter based on aOFETs.

3. References

1. F. Yang, L. Sun, J. Han, B. Li, X. Yu, X. Zhang, X. Ren, W. Hu, *ACS Appl. Mater. Interfaces*, 2018, **10**, 25871-25877.
2. S. Sung, S. Park, W. J. Lee, J. Son, C. H. Kim, Y. Kim, Y. N oh do, M. H. Yoon, *ACS Appl. Mater. Interfaces*, 2015, **7**, 7456-7461.
3. Q. Mu, Z. Chen, S. Duan, X. Zhang, X. Ren, W. Hu, *Front. Mater.*, 2020, **7**, 570002.
4. Y. Xi, T. Wang, Q. Mu, C. Huang, S. Duan, X. Ren, W. Hu, *Mater. Chem. Front.*, 2021, **5**, 3236-3245.
5. Q. Zhang, G. Xia, W. Xia, J. Z hou, S. Wang, *Synth. Met.*, 2015, **210**, 282-287.
6. D.-K. Kim, M. Lee, B. Kim, J.-H. Choi, *Org. Electron.,* 2019, **74**, 135-143.
7. J. D. Oh, J. W. Kim, D. K. Kim, J. H. Choi, *Org. Electron.*, 2016, **30**, 131-135.
8. Acton, G. Ting, H. Ma, J. W. Ka, H. L. Yip, N. M. Tucker, A. K. Y. Jen, *Adv. Mater.*, 2008, **20**, 3697-3701.
9. W. He, W. Xu, Q. Peng, C. Liu, G. Zhou, S. Wu, M. Zeng, Z. Zhang, J. Gao, X. Gao, et al., *J. of Phys. Chem. C*, 2016, **120**, 9949-9957.
10. J. Liu, H. Zhang, H. Dong, L. Meng, L. Jiang, L. Jiang, Y. Wang, J. Yu, Y. Sun, W. Hu, et al., *Nat. Commun.*, 2015, **6**, 10032.
11. Y. Ito, A. A. Virkar, S. Mannsfeld, J. H. Oh, M. Toney, J. Locklin, Z. Bao, *J. Am. Chem. Soc.*, 2009, **131**, 9396-9404.
12. K. Niimi, M. J. Kang, E. Miyazaki, I. Osaka, K. Takimiya, *Org. Lett.*, 2011, **13**, 3430-3433.
13. S. Duan, T. Wang, B. Geng, X. Gao, C. Li, J. Zhang, Y. Xi, X. Zhang, X. Ren, W. Hu, *Adv. Mater.*, 2020, **32**, 1908388.
14. S. Tatemichi, M. Ichikawa, T. Koyama, Y. Taniguchi, *Appl. Phys. Lett.*, 2006, **89**, 112108.
15. S. Guo, J. Yao, Y. Wang, L. Zhang, F. Zhai, X. Zhang, Y. Feng, W. Feng, X. Zhang, J. Jie, et al., *J. Mater. Chem. C*, 2021, **9**, 5758-5764.
16. S. P. Senanayak, V. K. Sangwan, J. J. McMorrow, K. Everaerts, Z. Chen, A. Facchetti, M. C. Hersam, T. J. Marks, K. S. Narayan, *Adv. Electron. Mater.*, 2015, **1**, 1500226.
17. H. Seong, J. Choi, B. C. Jang, M. Kim, S. Yoo, S. Y. Choi, S. G. Im, *Adv. Electron. Mater.*, 2016**, 2**, 1500385.
18. J. W. Kim, J. D. Oh, D. K. Kim, H. Y. Lee, Y. G. Ha, J. H. Choi, *J. Mater. Chem. C*, 2016, **4**, 7999-8005.
19. C. Lu, Z. Ji, G. Xu, N. Lu, L. Li, M. Liu, *Org. Electron.*, 2017, **49**, 206-211.
20. H. Jinno, T. Yokota, N. Matsuhisa, M. Kaltenbrunner, Y. Tachibana, T. Someya, *Org. Electron.*, 2017, **40**, 58-64.

21. U. Zschieschang, V. P. Bader, H. Klauk, *Org. Electron.*, 2017, **49**, 179-186.
22. F. C. Wu, B. L. Yeh, T. H. Chou, J. S. Chen, H. L. Cheng, W. Y. Chou, *Org. Electron.*, 2018, **59**, 374-381.
23. E. Stucchi, G. Dell'Erba, P. Colpani, Y.-H. Kim, M. Caironi, *Adv. Electron. Mater.,* 2018, **4**, 1800340.
24. Y. Takeda, Y. Yoshimura, R. Shiwaku, K. Hayasaka, T. Sekine, T. Okamoto, H. Matsui, D. Kumaki, Y. Katayama, S. Tokito, *Adv. Electron. Mater.,* 2018, **4**, 1700313.
25. T. Sawada, T. Makita, A. Yamamura, M. Sasaki, Y. Yoshimura, T. Hayakawa, T. Okamoto, S. Watanabe, S. Kumagai, J. Takeya, *Appl. Phys. Lett.,* 2020, **117**, 033301
26. .A. Petritz, A. Wolfberger, A. Fian, T. Griesser, M. Irimia-Vladu, B. Stadlober, *Adv. Mater.*, 2015, **27**, 7645-7656.
27. J. Liu, X. Gao, J. L. Xu, A. Ruotolo, S. D. Wang, *IEEE Electron Device Letters*, 2017, **38**, 1461-1464.
28. S. Tatemichi, M. Ichikawa, S. Kato, T. Koyama, Y. Taniguchi, *Phys. Stat. Sol. RRL*, 2008, **2**, 47-49.
29. S. C. Martens, U. Zschieschang, H. Wadepohl, H. Klauk, L. H. Gade, *Chem. Eur. J*. 2012, **18**, 3498-3509.
30. J. H. Park, Y. B. Yoo, K. H. Lee, W. S. Jang, J. Y. Oh, S. S. Chae, H. K. Baik, *Appl. Mater. Interfaces*, 2013, **5**, 410-417.
31. G. He, L. D. Zhang, G. W. Meng, G. H. Li, Q. Fang, J. P. Zhang, *J. Appl. Phys.*, 2007, **102**, 094103.
32. J. Gao, G. He, M. Liu, J. G. Lv, Z. Q. Sun, C. Y. Zheng, P. Jin, D. Q. Xiao, X. S. Chen, *J. Alloys Compd.*, 2017, **691**, 504-513.